Eur. Phys. J. E (2018) **41**: 23
DOI 10.1140/epje/i2018-11628-5

THE EUROPEAN PHYSICAL JOURNAL E

Regular Article

Stability of a stationary plane-parallel flow of a ternary fluid between two vertical plates maintained at constant different temperatures*

T. Lyubimova[1,2,a], N. Lobov[2], and V. Shevtsova[1,3]

[1] Computational Fluid Dynamics Laboratory, Institute of Continuous Media Mechanics UB RAS, Perm, Russia
[2] Theoretical Physics Department, Perm State University, Perm, Russia
[3] MRC, CP-165/62, Université Libre de Bruxelles (ULB), Brussels, Belgium

Received 13 October 2017 and Received in final form 18 January 2018
Published online: 16 February 2018 –

Abstract. The linear stability of a steady convective flow of a ternary mixture placed between differently heated vertical rigid plates is studied. The applied temperature gradient induces concentration gradients due to the Soret effect. The analysis is done for the case when separation ratios of ternary mixture, *i.e.*, Soret coefficients, have different signs but the net separation ratio is negative. The stability maps in terms of the Grashof number and net separation ratio are obtained and discussed for monotonic and oscillatory modes of instability. The previous results for long-wave instability of a binary mixture were recovered in the limit when one of the Soret coefficients tends to zero. For finite-wavelength perturbations the previous results were extended by discovering the oscillatory instability.

Introduction

Convection plays an important role in many natural and technological processes such as ocean flows, distribution of components in hydrocarbon reservoirs, the growth of crystals, the solidification of metallic alloys and others. Many natural gases and liquids consist of several components. Due to the complex composition, transport processes (thermal diffusion, molecular diffusion and thermal conductivity) in such mixtures are much more complex than in binary mixtures. Thermal diffusion (also thermodiffusion or the Soret effect) is a molecular transport of substance caused by a thermal gradient. In binary mixtures, one can distinguish between the positive Soret effect, when the lighter (heavier) component is driven towards the higher (lower) temperature region, and the negative Soret effect, when the situation is the opposite. The reciprocal phenomenon to the Soret effect is the Dufour effect, *i.e.* thermal transport due to a mass concentration gradient.

In one of the first works on convection in binary mixtures [1] with the Soret and Dufour effects the case of a plane horizontal layer subjected to a vertical temperature gradient was studied numerically. It was found that in the case of positive Soret effect there exists only monotonic instability for heating from below, and the convectionless state instability threshold decreases in comparison with the single-component fluid. In the case of negative Soret effect and heating from below the oscillatory instability is possible. In this case a lighter component is accumulated in the upper part of the layer which increases the instability threshold of the convectionless state. Monotonic instability arises in the case of negative Soret effect at heating from above. In [2] a linear stability analysis was made for the case of constant heat flux, long-wave and short-wave instabilities were studied for positive Soret effect and heating from below.

The stability of steady plane-parallel convective flows of binary mixture between two rigid vertical plates maintained at constant different temperatures was studied taking into account the Soret effect but neglecting the Dufour effect in [3,4]. Three instability mechanisms were observed. In [5] the stability of steady plane-parallel convective flows of binary mixture with the Soret effect between two rigid vertical plates kept at constant different temperatures in the presence of a vertical temperature stratification was studied by the Galerkin method. The calculations were performed for two positive values of separation ratio when the Prandtl number and Schmidt number range from 0.01 to 10. A hydrodynamic instability mode takes place for the parameter range covered in the calculations. In [6], a similar problem was studied for a wider range of parameters and thermosolutal instability modes were found.

* Contribution to the Topical Issue "Non-equilibrium processes in multicomponent and multiphase media" edited by Tatyana Lyubimova, Valentina Shevtsova, Fabrizio Croccolo.

[a] e-mail: lubimova@psu.ru

The problem of the stability of convective flows in mixtures with three or more components is poorly studied even in the absence of the Soret effect. An experimental study of the stability of a ternary gaseous mixture in a vertical channel was carried out in [7]. The channel connected two flasks. The upper flask was filled with a mixture of light and heavy gases, the lower one by gas. The density of the mixture in the upper flask was smaller than the density of the gas in the lower flask. Convection developed in the channel.

The phenomenon of diffusion barrier which arises in mixtures with different properties of mutual diffusion of components was investigated in [8]. The increase of pressure in the lower flask under the action of baroeffect results in the development of flow of the mixture from the lower flask to the upper one with the velocity substantially exceeding the rate of diffusion of one of the components. As a result, the distribution of concentrations in the channel becomes nonlinear and the density inversion appears which leads to the development of the Rayleigh-Taylor instability.

The stability of a convective flow of a binary mixture in a vertical layer was studied in [9] taking into account thermodiffusion effect. At weak thermodiffusion a monotonic instability occurs related to the development of vortices at the boundary of counter flows. At positive Soret effect the instability threshold is lowered due to the increase of the base flow velocity. At negative Soret effect the increase of the instability threshold was reported.

Long-wave instability of steady convective flows of ternary mixtures between two vertical rigid plates kept at constant different temperatures was studied in [10]. It was shown analytically (by expansion into series of small wave number) that there exist monotonic and oscillatory long-wave instability modes. The onset and nonlinear regimes of the Soret-induced convection of ternary mixtures in a square cavity at different levels of gravity were studied in [11,12].

In the present paper the instability mechanisms of a steady plane-parallel convective flow of a ternary mixture between two vertical rigid plates kept at constant different temperatures are studied numerically with respect to finite-wavelength perturbations.

Problem formulation: governing equations

Let us consider a ternary mixture of non-reacting components between two infinite vertical rigid plates separated by the distance $2h$, *i.e.* $-h \le x \le h$ where x is the horizontal coordinate in the direction perpendicular to the layer boundaries. The layer boundaries are perfectly conductive, they are maintained at constant different temperatures $T = \mp\theta$. The mass flux through the boundaries is absent.

We assume that the mixture density is a linear function of temperature and concentrations of components $C_{1,2}$:

$$\rho = \rho_0(1 - \beta T - \beta_1 C_1 - \beta_2 C_2).$$

Here ρ_0 is the density of a mixture at the mean values of temperature and concentrations; T and C_1, C_2 are small deviations of temperature and concentrations from the mean values; β is the thermal expansion coefficient, β_1, $\beta_2 > 0$ are the solutal expansion coefficients.

We apply the Boussinesq approximation. The Dufour effect is not taken into account. The governing equations for a ternary mixture in Boussinesq approximation have the form:

$$\frac{\partial \vec{v}}{\partial t} + (\vec{v}\nabla)\vec{v} = -\frac{1}{\rho_0}\nabla p + \nu \Delta \vec{v} - \vec{g}(\beta T + \vec{I}\cdot B\vec{C}), \quad (1)$$

$$\frac{\partial T}{\partial t} + (\vec{v}\nabla)T = \chi \Delta T, \quad (2)$$

$$\frac{\partial \vec{C}}{\partial t} + (\vec{v}\nabla)\vec{C} = D\Delta\vec{C} + \vec{D}_T \Delta T, \quad (3)$$

$$\nabla \cdot \vec{v} = 0. \quad (4)$$

Here $\vec{v}$ and p are the velocity and pressure, ν is the kinematic viscosity, χ is the thermal diffusivity coefficient, $\vec{g}$ is the gravitational acceleration, $\vec{I} = (1,1)$ is the vector, the dimension of which equals the number of independent components, $B = \left(\begin{smallmatrix} \beta_1 & 0 \\ 0 & \beta_2 \end{smallmatrix}\right)$ is the diagonal matrix of solutal expansion coefficients, $\vec{C} = (C_1, C_2)$ is the vector of concentrations, $D = \left(\begin{smallmatrix} D_{11} & D_{12} \\ D_{21} & D_{22} \end{smallmatrix}\right)$ is the matrix of the molecular diffusion coefficients, and $\vec{D}_T$ is the vector of thermodiffusion coefficients related to the vector of the Soret coefficients $\vec{S}_T$ by the relation $\vec{S}_T = D^{-1}\vec{D}_T$.

At the layer boundaries $x = \pm h$ the no-slip conditions are imposed

$$\vec{v} = 0, \quad (5)$$

the constant different temperatures are maintained

$$T = \mp\theta \quad (6)$$

and the mass flux through the boundaries is absent:

$$D\frac{\partial \vec{C}}{\partial x} + \vec{D}_T \frac{\partial T}{\partial x} = 0. \quad (7)$$

Additionally, the presence of rigid walls at the top and bottom implies that the flow rate through every cross-section of constant x must be zero:

$$\int_{-h}^{h} v_z \mathrm{d}x = 0. \quad (8)$$

To simplify eqs. (1)–(4) it is convenient to exclude the coefficients of cross-diffusion (*i.e.*, D_{12}, D_{21}). It was suggested in [13] to transform the matrix of molecular diffusion coefficients to diagonal form by means of the transformation $\tilde{D} = V^{-1}DV$, where $\tilde{D}$ is the diagonal matrix formed by the eigenvalues of the matrix D, V is the matrix, whose columns represent the eigenvectors $\vec{s}_i = (s_{i1}, s_{i2})$ of the matrix D, $i = 1, 2$. Here an additional matrix is introduced

$$Q = \mathrm{diag}\{q_1, q_2\}, \qquad q_i = \beta_i^{-1}\sum_{j=1}^{2}\beta_j s_{ij} \quad (9)$$

and concentrations and thermodiffusion coefficients are replaced according to the formulas

$$\vec{C} = VQ^{-1}\vec{\tilde{C}}, \qquad \vec{D}_T = VQ^{-1}\vec{\tilde{D}}_T. \tag{10}$$

It is assumed that the transformation is reversible and $q_i \neq 0$, thus $\det Q \neq 0$. Applying the transformation to the equations and boundary conditions, we obtain

$$\frac{\partial \vec{v}}{\partial t} + (\vec{v}\nabla)\vec{v} = -\frac{1}{\rho_0}\nabla p + \nu\Delta\vec{v} - \vec{g}(\beta T + \vec{I}\cdot B\tilde{C}), \tag{11}$$

$$\frac{\partial T}{\partial t} + (\vec{v}\nabla)T = \chi\Delta T, \tag{12}$$

$$\frac{\partial \vec{\tilde{C}}}{\partial t} + (\vec{v}\nabla)\vec{\tilde{C}} = \tilde{D}\Delta\vec{\tilde{C}} + \vec{\tilde{D}}_T\Delta T, \tag{13}$$

$$\nabla\cdot\vec{v} = 0, \tag{14}$$

$$x = \pm h: \quad \vec{v} = 0, \quad T = \mp\theta, \quad \tilde{D}\frac{\partial\vec{\tilde{C}}}{\partial x} + \vec{\tilde{D}}_T\frac{\partial T}{\partial x} = 0, \tag{15}$$

$$\int_{-h}^{h} v_z \mathrm{d}x = 0. \tag{16}$$

As the result of transformation the number of parameters is reduced; this simplifies the problem.

Let us write the governing equations (11)–(14) and boundary conditions (15), (16) in dimensionless form introducing the following scales: length (h), time (h^2/ν), velocity ($g\beta\theta h^2/\nu$), temperature (θ), concentration ($\beta\theta/\beta_{1,2}$). To simplify the notations, the "tilde" will be dropped:

$$\frac{\partial\vec{v}}{\partial t} + \mathrm{Gr}(\vec{v}\nabla)\vec{v} = -\nabla p + \Delta\vec{v} + (T + C_1 + C_2)\vec{\gamma}, \tag{17}$$

$$\frac{\partial T}{\partial t} + \mathrm{Gr}(\vec{v}\nabla)T = \mathrm{Pr}^{-1}\Delta T, \tag{18}$$

$$\frac{\partial C_{1,2}}{\partial t} + \mathrm{Gr}(\vec{v}\nabla)C_{1,2} = \mathrm{Sc}_{1,2}^{-1}(\Delta C_{1,2} - \varepsilon_{1,2}\Delta T), \tag{19}$$

$$\nabla\cdot\vec{v} = 0. \tag{20}$$

At $x = \pm 1$:

$$\vec{v} = 0, \tag{21}$$

$$T = 0, \tag{22}$$

$$C'_{1,2} - \varepsilon_{1,2}T' = 0. \tag{23}$$

Additionally

$$\int_{-1}^{1} v_z \mathrm{d}x = 0. \tag{24}$$

Here $\varepsilon_{1,2} = -\alpha_{1,2}\beta_{1,2}/\beta D_{1,2}$ are the dimensionless separation ratios, $\alpha_{1,2}$ are the thermodiffusion coefficients of first and second solutes, $D_{1,2}$ are the molecular diffusion coefficients (elements of the diagonal matrix $D_{11} = D_1$, $D_{22} = D_2$), $\vec{\gamma}$ is the unit vector directed vertically upward. For positive Soret effect $\alpha_{1,2} < 0$, $\varepsilon_{1,2} > 0$, for negative Soret effect $\alpha_{1,2} > 0$, $\varepsilon_{1,2} < 0$.

The problem contains the following dimensionless parameters: the Grashof number Gr, the Prandtl number Pr, the Schmidt numbers $\mathrm{Sc}_{1,2}$:

$$\mathrm{Gr} = \frac{g\beta_1\theta h^3}{\nu^2}, \qquad \mathrm{Pr} = \frac{\nu}{\chi}, \qquad \mathrm{Sc}_{1,2} = \frac{\nu}{D_{1,2}}.$$

The problem under consideration has the solution which corresponds to the plane-parallel steady flow in vertical direction with cubic velocity profile and linear distributions of temperature and concentrations of solutes. This basic state in dimensionless form is given by

$$v_0 = \frac{1+\varepsilon}{6}(x^3 - x), \qquad T_0 = -x,$$
$$C_{01} = -\varepsilon_1 x, \qquad C_{02} = -\varepsilon_2 x. \tag{25}$$

Here $\varepsilon = \varepsilon_1 + \varepsilon_2$ is the net separation ratio.

Stability problem

To study the linear stability of the base flow we represent all the fields as sums of basic state and small perturbations:

$$\vec{v} = \vec{v}_0 + \vec{v}', \qquad T = T_0 + T',$$
$$p = p_0 + p', \qquad C = C_0 + C'.$$

The mathematical model in the current study is limited to two-dimensional perturbations depending only on x and z coordinates and time. In this case it is convenient to introduce the stream function by the relations

$$v_x = -\frac{\partial\psi}{\partial z}, \qquad v_z = \frac{\partial\psi}{\partial x}.$$

The linearized equations for perturbations in terms of stream function, temperature and concentrations have the form

$$\frac{\partial}{\partial t}\Delta\psi + v_0\mathrm{Gr}\frac{\partial}{\partial z}\Delta\psi - v_0''\mathrm{Gr}\frac{\partial\psi}{\partial z} = \Delta\Delta\psi + \frac{\partial T}{\partial x} + \frac{\partial}{\partial x}(C_1 + C_2), \tag{26}$$

$$\frac{\partial T}{\partial t} + v_0\mathrm{Gr}\frac{\partial T}{\partial z} - \mathrm{Gr}\frac{\partial T_0}{\partial x}\frac{\partial\psi}{\partial z} = \frac{1}{\mathrm{Pr}}\Delta T, \tag{27}$$

$$\frac{\partial C_{1,2}}{\partial t} + v_0\mathrm{Gr}\frac{\partial C_{1,2}}{\partial z} - \mathrm{Gr}\frac{\partial C_{01,2}}{\partial x}\frac{\partial\psi}{\partial z} = \frac{1}{\mathrm{Sc}_{1,2}}\Delta(C_{1,2} - \varepsilon_{1,2}T). \tag{28}$$

The boundary conditions are rewritten as

$$\frac{\partial\psi}{\partial x} = 0, \qquad \frac{\partial\psi}{\partial z} = 0, \tag{29}$$

$$T = 0, \tag{30}$$

$$C'_{1,2} - \varepsilon_{1,2}T' = 0. \tag{31}$$

We consider the perturbations in the form of normal modes:

$$\psi(x,z) = \varphi(x)e^{-\lambda t+ikz},$$
$$T(x,z) = \vartheta(x)e^{-\lambda t+ikz},$$
$$C_{1,2}(x,z) = \xi_{1,2}(x)e^{-\lambda t+ikz}.$$

The problem of the linear stability of the base solution (25) to the plane normal mode perturbations has the form

$$-\lambda\Delta\varphi+v_0ik\mathrm{Gr}\Delta\varphi-v_0''ik\mathrm{Gr}\varphi=\Delta\Delta\varphi+(\vartheta'+\xi_1'+\xi_2'), \quad (32)$$

$$-\lambda\vartheta + v_0ik\mathrm{Gr}\vartheta - T_0'ik\mathrm{Gr}\varphi = \frac{1}{\mathrm{Pr}}\Delta\vartheta, \quad (33)$$

$$-\lambda\xi_{1,2} + v_0ik\mathrm{Gr}\xi_{1,2} - C_{01,2}'ik\mathrm{Gr}\varphi = \frac{1}{\mathrm{Sc}_{1,2}}\Delta(\xi_{1,2} - \varepsilon_{1,2}\vartheta), \quad (34)$$

$$x = \pm 1: \qquad \varphi = 0, \qquad \varphi' = 0, \quad (35)$$
$$\vartheta = 0, \quad (36)$$
$$\xi_{1,2}' - \varepsilon_{1,2}\vartheta' = 0. \quad (37)$$

Here $\lambda = \lambda_r + i\omega$ is the complex growth rate of perturbations, k is the wave number, the prime denotes differentiation with respect to the x coordinate, and Δ is the two-dimensional Laplace operator.

The problem (32)–(37) was solved by the differential sweep method applied for the first time to the hydrodynamic stability problem in [14].

Numerical results

A numerical study was performed for fixed values of Prandtl and Schmidt numbers $\mathrm{Pr} = 10$, $\mathrm{Sc}_1 = 1390$, $\mathrm{Sc}_2 = 2244$, while separation ratios ε_1, ε_2 were varied.

First, we consider the stability of a binary mixture by assuming that $\varepsilon_1 = 0$ ($\varepsilon = \varepsilon_2$). Figure 1 presents the stability map for this case comparing different types of instability. In all the figures the notation $\mathrm{Gr_m}$ corresponds to the minimal critical value of the $\mathrm{Gr}(k)$. It follows that in this case, at small negative net separation ratios ($-0.14 < \varepsilon < 0$) the crisis of stationary plane-parallel flow is caused by the hydrodynamic instability mode (curve 4, right branch) which has a non-viscous nature, and is related to the presence of the inflection point in the velocity profile. The calculations showed that this monotonic finite-wavelength instability mode develops in the form of immovable vortices at the boundary of upstream and downstream flows. At $\varepsilon = 0$ the concentration gradient is absent and the mixture behaves as a single-component fluid, the right curve 4 intersects the Gr axis at ≈ 492. With the increase of $|\varepsilon|$ the base flow velocity changes as $(1 + \varepsilon)$ which results in the stability growth at $-1 < \varepsilon < 0$ up to absolute stabilization at $\varepsilon = -1$. There is the second branch of the hydrodynamic instability mode at $\varepsilon < -1$ (curve 4, left branch) but in the range of ε under consideration it is not the most dangerous.

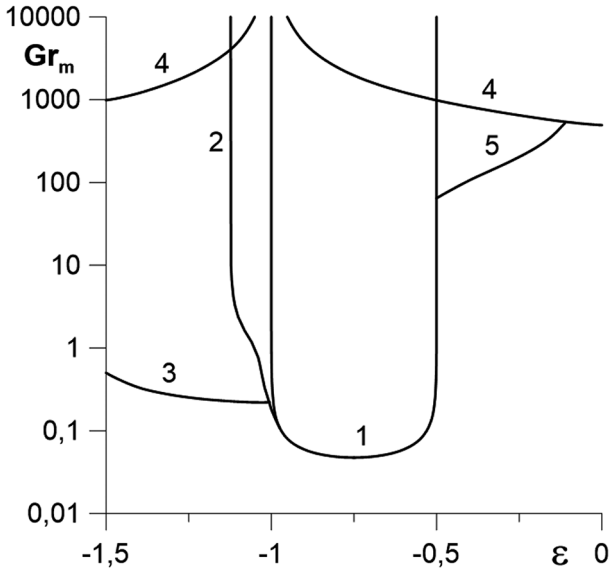

Fig. 1. Stability map for $\mathrm{Pr} = 10$, $\mathrm{Sc}_1 = 1390$, $\mathrm{Sc}_2 = 2244$, $\varepsilon_1 = 0$; 1 —long-wave monotonic thermosolutal instability mode, 2 —finite-wavelength monotonic thermosolutal instability mode, 3 —finite-wavelength oscillatory thermosolutal instability mode, 4 —finite-wavelength monotonic hydrodynamic instability mode, 5 —concentrational waves.

With the increase of $|\varepsilon|$, an instability mode related to the growing oscillatory perturbations becomes the most dangerous (line 5 in fig. 1). There are two waves propagating in upward and downward directions with phase velocities close to the maximal velocities of the base flow. The nature of these waves depends on Prandtl and Schmidt number values (see [3]), they can be thermal, solutal or mixed. For the Prandtl and Schmidt number values under consideration, typical for liquid mixtures, these waves have the solutal nature. The solutal wave remains the most dangerous instability mode at $-0.5 < \varepsilon < -0.14$.

At $\varepsilon = -0.5$ the monotonic thermosolutal instability mode becomes the most dangerous (curve 1 in fig. 1). The critical Grashof number for this mode is small enough, *i.e.* strong destabilization of the base flow takes place. The appearance of a thermosolutal instability mechanism at negative Soret effect is related to the presence of horizontal temperature and concentration gradients directed opposite to each other and to the difference in relaxation time scales of thermal and solutal perturbations [3,9]. In this case, if a liquid element is displaced in horizontal direction, its density becomes different from the density of the surrounding liquid. This leads to the appearance of buoyancy force which causes the motion of the liquid element in vertical direction and can result in the development of instability. The base flow crisis for this mode is caused by the development of long-wave perturbations. This is related to the absence of mass flux through the boundaries, because of that solutal perturbations developing near the boundaries have a large scale in longitudinal direction.

The global minima of neutral curves for thermosolutal perturbations remain located at $k = 0$, *i.e.* long-wave

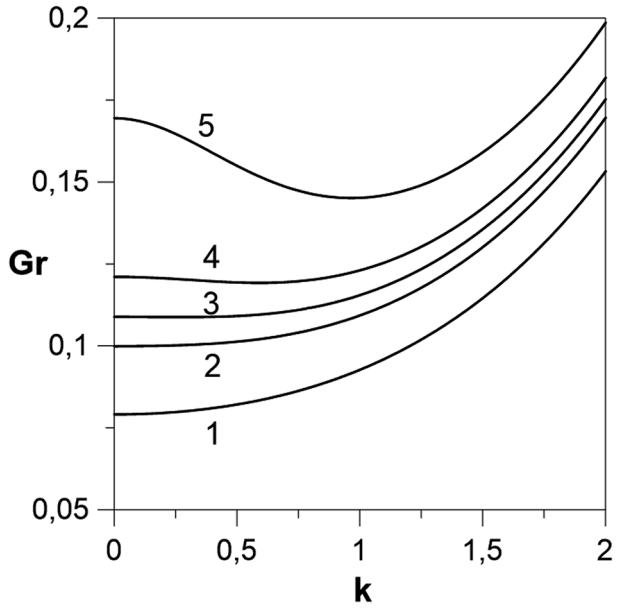

Fig. 2. Transition from the long-wave to finite-wavelength thermosolutal monotonic instability mode: Pr = 10, Sc_1 = 1390, Sc_2 = 2244, $\varepsilon_1 = 0$, $\varepsilon = -0.95, -0.97, -0.975, -0.98, -0.99$ (curves 1–5, respectively).

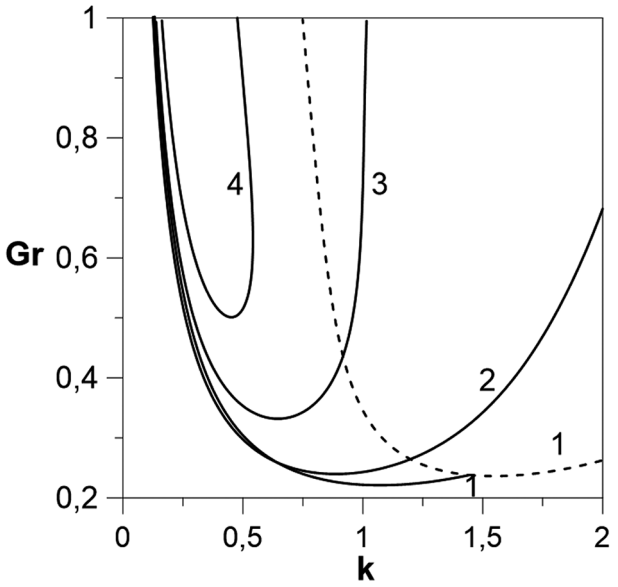

Fig. 3. Branching oscillatory finite-wavelength thermosolutal instability mode from the monotonic finite-wavelength thermosolutal instability mode: $\varepsilon_1 = 0$, Pr = 10, Sc_1 = 1390, Sc_2 = 2244, $\varepsilon = -1.01, -1.2, -1.4, -1.5$ (curves 1–4, respectively).

perturbations remain the most dangerous, in a wide range of net separation ration $\varepsilon < -0.5$. However, at $\varepsilon < -0.98$ the global minima of neutral curves for this instability mode correspond to non-zeroth k, *i.e.* the finite-wavelength perturbations become the most dangerous (see fig. 2 that illustrates the transition from the long-wave to finite-wavelength thermosolutal perturbations). The dependence of the critical Grashof which corresponds to the global (finite-wavelength) minimum on the net separation ratio is shown in fig. 1 by the curve 2. The points at the curve 1 located above the branching curve 2 from curve 1 show only the values of the Grashof number which correspond to the neutral monotonic perturbations with $k = 0$. These perturbations are not the most dangerous anymore.

The calculations carried out at $\varepsilon < -1$ have also shown the appearance of an oscillatory finite-wavelength thermosolutal instability mode (curve 3 in fig. 1) soon after the branching of the monotonic finite-wavelength thermosolutal instability mode (curve 2 in fig. 1) from the long-wave monotonic thermosolutal instability mode (curve 1 in fig. 1). It occurs at $\varepsilon \approx -1.01$ as illustrated by dashed and solid curves 1 in fig. 3. As a result, the crisis of the base flow at $\varepsilon < -1.01$ is attributed to the development of oscillatory finite-wavelength thermosolutal perturbations. A comparison of the neutral curves 1–4 in fig. 3 shows that the instability threshold to the oscillatory finite-wavelength thermosolutal perturbations increases with the decrease of ε. The neutral curves of the monotonic finite-wavelength thermosolutal instability for $\varepsilon < -1.01$ are not shown in fig. 3, as one can see from fig. 1, the minima of these neutral curves are located higher than those of oscillatory finite-wavelength thermosolutal neutral curves. It is worth mentioning that the oscillatory

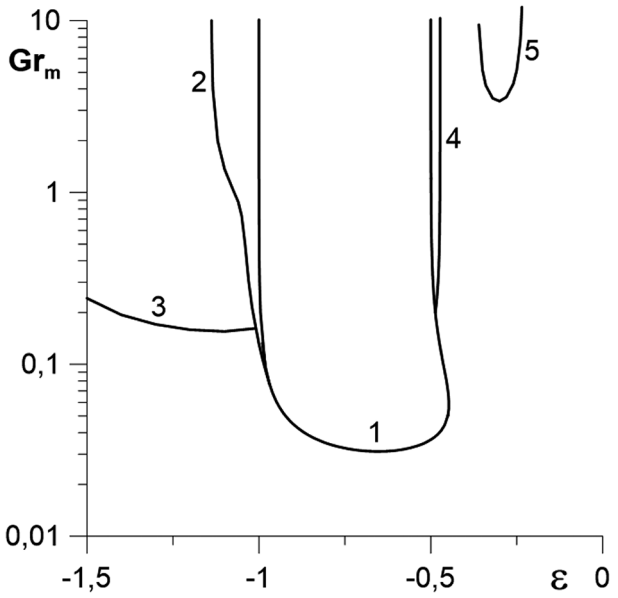

Fig. 4. Stability map for Pr = 10, Sc_1 = 1390, Sc_2 = 2244, ε_1 = 1: 1 —long-wave monotonic thermosolutal instability mode, 2 —finite-wavelength monotonic thermosolutal instability mode, 3 —finite-wavelength oscillatory thermosolutal instability mode, 4 —long-wave thermosolutal oscillatory instability mode, 5 —finite-wavelength oscillatory thermosolutal instability mode.

finite-wavelength thermosolutal instability mode was not found in [9].

The stability map for the ternary mixture with $\varepsilon_1 = 1$ is shown in fig. 4. As one can see, the instability thresholds to all perturbations are lower than for $\varepsilon_1 = 0$ (the insta-

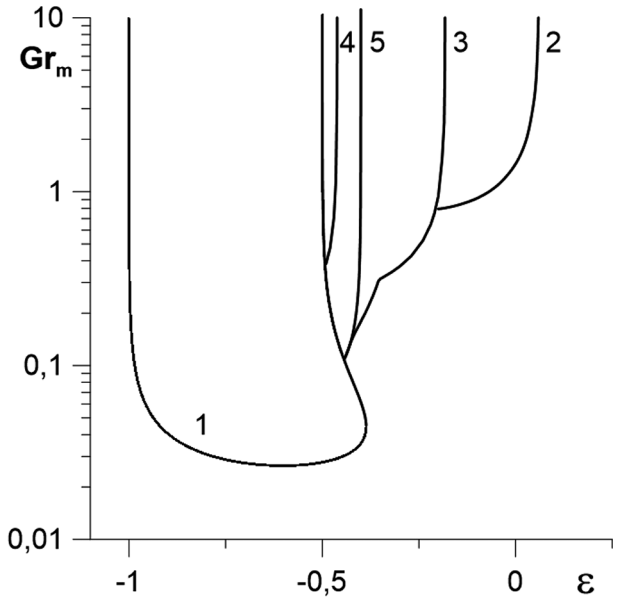

Fig. 5. Stability map for Pr = 10, $Sc_1 = 1390$, $Sc_2 = 2244$, $\varepsilon_1 = 1.5$: 1 —long-wave monotonic thermosolutal instability mode, 2, 3, 4 —finite-wavelength oscillatory thermosolutal instability modes, 5 —long-wave oscillatory thermosolutal instability mode.

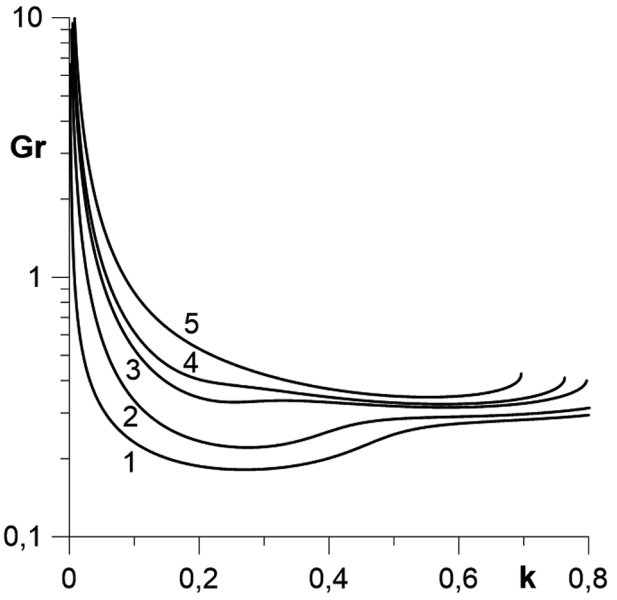

Fig. 6. Neutral curves of the oscillatory finite-wavelength thermosolutal instability mode for Pr = 10, $Sc_1 = 1390$, $Sc_2 = 2244$, $\varepsilon_1 = 1.5$; $\varepsilon = -0.399, -0.38, -0.35, -0.34, -0.32$, curves 1–5, respectively.

bility boundary to concentrational waves depends only on the net separation ratio, its location is the same as for $\varepsilon_1 = 0$ and is not shown in fig. 4). Moreover, the monotonic long-wave thermosolutal instability becomes possible at $\varepsilon > -0.5$ (curve 1). An additional domain of instability to oscillatory finite-wavelength thermosolutal perturbations appears at $-0.363 < \varepsilon < -0.232$.

At $\varepsilon_1 = 1$ there exists the oscillatory long-wave thermosolutal instability mode found in [13] (curve 4). This mode does not exist in a binary mixture when $\varepsilon_1 = 0$ and in a ternary mixture at $\varepsilon_1 = 1$ it exists in a rather narrow range of net separation ratio values. The existence of the oscillatory long-wave mode is related to the mass flux vanishing at the rigid boundaries for two solutes, because of that solutal perturbations of two types developing near the layer boundaries have large scale in longitudinal direction.

In fig. 5 the stability map is plotted for $\varepsilon_1 = 1.5$. From a comparison of figs. 4 and 5, at $\varepsilon_1 = 1.5$ it follows that the size of the additional domain of the oscillatory finite-wavelength thermosoloutal instability (curve 3 in fig. 4) becomes larger and its boundary splits into three parts. Two of them join the boundary of the domain of the monotonic long-wave thermosolutal instability (the corresponding neutral curves branch from the neutral curve of the long-wave mode). The third part (curve 2) is shifted to the positive values of net separation ratio. The splitting of the curve 3 is related to the appearance of two minima at neutral curves and their competition which is illustrated by fig. 6. At the splitting point the jumps of the wave number and frequency occur which is shown in fig. 8 (curve 2). A long-wave monotonic thermosolutal instability mode exists at even larger values of the parameter ε than at $\varepsilon_1 = 1$.

Curve 5 in fig. 5 shows the boundary of the long-wave oscillatory thermosolutal instability mode. As one can see, at $\varepsilon_1 = 1.5$ this mode exists in a wider range of net separation ratio than at $\varepsilon_1 = 1$ but in most part of its existence range it is less dangerous than the finite-wavelength oscillatory thermosolutal instability mode.

The neutral curves of the long-wave monotonic and oscillatory thermosolutal instability modes for $\varepsilon = -0.425$ are presented in fig. 7(a). The oscillation frequency is positive, it grows with the increase of Gr (fig. 7(b)).

In fig. 8(a) the dependence of the wave number of the most dangerous perturbations k_m on the net separation ratio ε is plotted for three boundaries of the oscillatory finite-wavelength thermosolutal instability found at $\varepsilon_1 = 1.5$ (curves 2, 3, 4 in fig. 5). For two boundaries (curves 1 and 3 in fig. 8(a)) the wavelength decreases with the increase of the net separation ratio and for the boundary with a break (curve 2 in fig. 8(a)) the behaviour is more complex.

The frequency of the most dangerous perturbations (fig. 8(b)) grows with the increase of net separation ratio. Each change of the instability mode is accompanied by a frequency skip.

Conclusions

The stability of a stationary plane-parallel convective flow of a ternary mixture in a vertical layer is studied. Stability maps in the parameter space in terms of the net separation ratio and Grashof number are obtained for the Schmidt

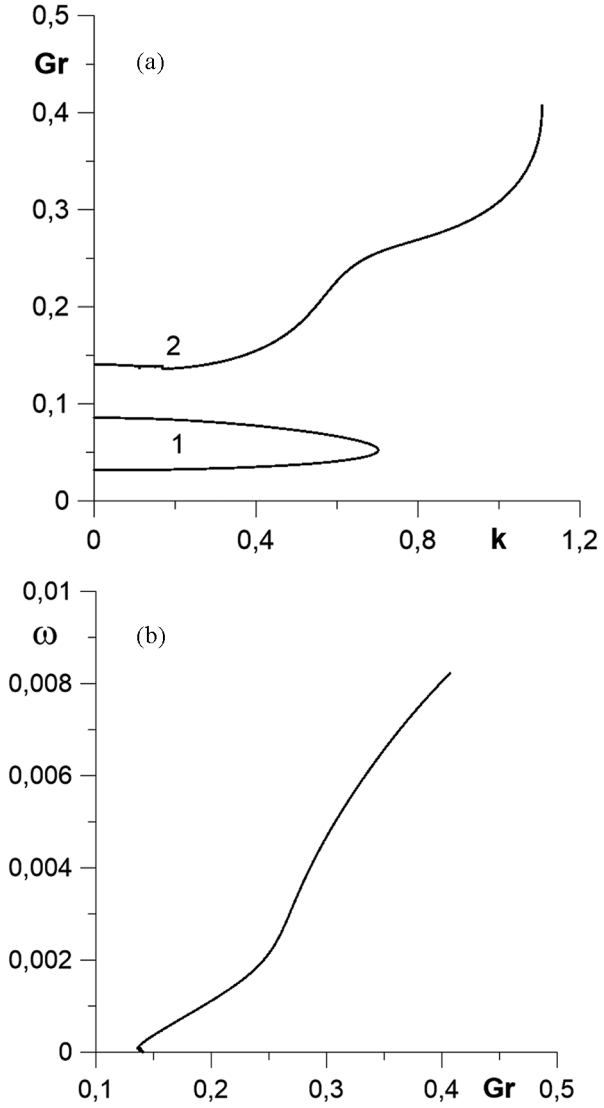

Fig. 7. Neutral curves for monotonic (curve 1) and oscillatory (curve 2) thermosolutal instability modes (a) and the dependence of the perturbation frequency on the Grashof number (b) for Pr = 10, $Sc_1 = 1390$, $Sc_2 = 2244$, $\varepsilon_1 = 1.5$, $\varepsilon = -0.425$.

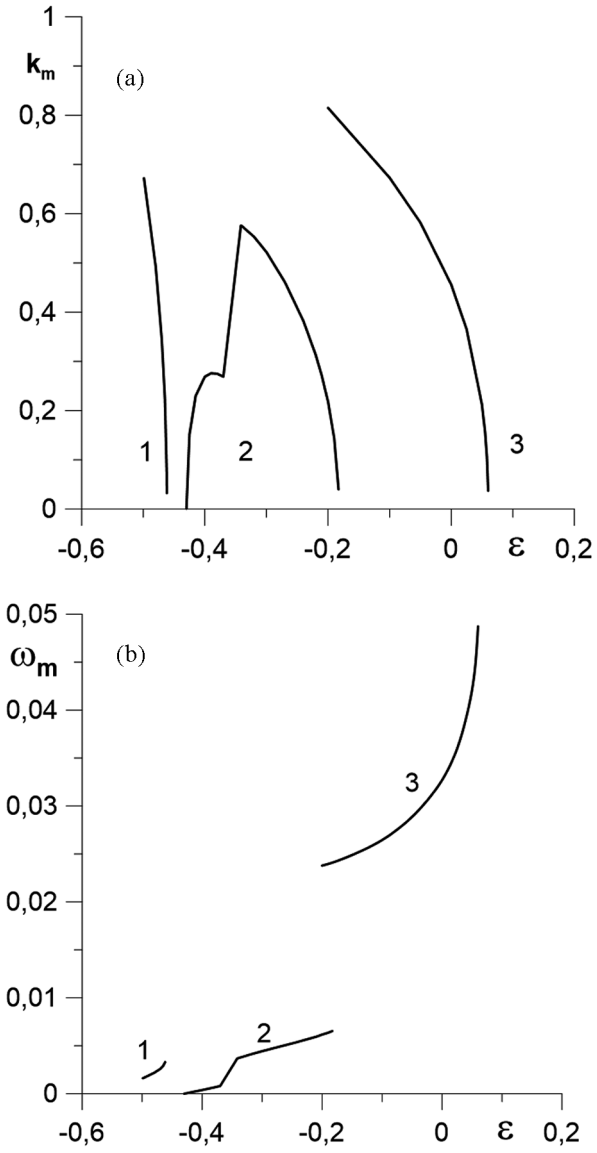

Fig. 8. Dependence of the wave number (a) and frequency (b) of the most dangerous perturbations on the net separation ratio ε: Pr = 10, $Sc_1 = 1390$, $Sc_2 = 2244$, $\varepsilon_1 = 1.5$; 1, 2, 3 —finite-wavelength oscillatory thermosolutal instability modes (they correspond to curves 4, 3 and 2, respectively, in fig. 5).

and Prandtl number values typical for liquid mixtures. The results of the stability analysis are presented for a ternary mixture when two corresponding separation ratios have different signs and for a binary mixture assuming that one of the values of the separation ratios is equal to zero. Taking into account the multi-parametric nature of the problem, the positive separation ratio is kept constant while the net separation ratio is changed. It is found that depending on the net separation ratio value the base flow crisis can be related to different instability mechanisms. At small values of $|\varepsilon|$ the finite-wavelength monotonic instability mode of hydrodynamic nature is responsible for the base flow crisis. With the increase of $|\varepsilon|$ the oscillatory finite-wavelength growing perturbations having the nature of the solutal waves propagating in opposite directions become the most dangerous. At even higher $|\varepsilon|$ the long-wave monotonic instability mode of thermosolutal nature (caused by thermodiffusion effect) is the most dangerous. With a further growth of $|\varepsilon|$ the finite-wavelength thermosolutal instability mode branches from the long-wave thermosolutal instability mode (the minima of neutral curves at $k = 0$ stop to be the global minima) and dominates.

A new oscillatory thermosolutal instability mode is discovered at the net separation ratio values $\varepsilon < -1$. It branches from the finite-wavelength monotonic thermosolutal instability mode.

All mentioned-above instability modes also exist in binary mixtures. The results obtained in the present work allow to observe the contribution of the second solute.

It is known that in the presence of two factors provoking the long-wave instability, the oscillatory long-wave instability arises [15,16]. In the problem under consideration these factors are the mass flux vanishing at rigid boundaries for two solutes. Indeed, the oscillatory long-wave thermosolutal instability mode for ternary fluids was found in [10]. The calculations carried out in the present work have shown that this mode exists in a narrow range of ε close to -0.5 and it remains more dangerous than the finite-wavelength oscillatory thermosolutal instability mode (the global minima of neutral curves correspond to $k = 0$) in a rather narrow range of its existence.

The work was supported by Russian Science Foundation (grant 14-21-00090).

Author contribution statement

T. Lyubimova contributed to the problem formulation, methodology of the investigation, numerical simulation, analysis and interpretation of numerical results, preparation of the draft and revision of the paper, she also works as corresponding author. N. Lobov contributed to the numerical simulation, analysis of numerical results and preparation of the draft of the paper. V. Shevtsova contributed to the problem formulation, analysis of numerical results, preparation of the draft and revision of the paper.

References

1. D.T.J. Hurle, E. Jakeman, J. Fluid Mech. **47**, 667 (1971).
2. E. Knobloch, D.R. Moore, Phys. Rev. A. **37**, 860 (1988).
3. G.Z. Gershuni, E.M. Zhukhovitsky, A.A. Nepomnyashchy, *Stability of Convective Flows* (Nauka, Moscow, 1989).
4. J.K. Platten, J.C. Legros, *Convection in Liquids* (Springer, Berlin, 1984).
5. B.I. Nikolaev, A.A. Tubin, Prikl. Mat. Mek. **35**, 248 (1971).
6. L.E. Sorokin, *Stability of convective flow of binary mixture in the presence of thermodiffusion and vertical concentration gradient*, in *Convective Flows* (PSPU, Perm, 1983) pp. 63–71.
7. V.N. Kosov, V.D. Seleznev, Yu.I. Zhavrin, Teplofiz. Aeromekh. **7**, 127 (2000).
8. Yu.I. Zhavrin, V.N. Kosov, V.D. Seleznev, Fluid Dyn. **35**, 464 (2000).
9. G.Z. Gershuni, E.M. Zhukhovitskii, L.E. Sorokin, J. Appl. Math. Mech. **46**, 54 (1982).
10. I.I. Ryzhkov, V.M. Shevtsova, Phys. Fluids **21**, 014102 (2009).
11. T.P. Lyubimova, N.A. Zubova, Micrograv. Sci. Technol. **26**, 241 (2014).
12. T.P. Lyubimova, N.A. Zubova, Eur. Phys. J. E **38**, 19 (2015).
13. I.I. Ryzhkov, V.M. Shevtsova, Phys. Fluids **19**, 0271101 (2007).
14. M.A. Goldshtik, V.A. Sapozhnikov, V.A. Shtern, *Differential factorisation method in problems of hydrodynamic stability*, *Proceedings of the GAMM Conference on Numerical Methods in Fluid Mechanics, Oct. 1975, Cologne* (DVFLR Institut für Angewandte Gasdynamik, Porz-Wahn, 1975) pp. 52–58.
15. T.P. Lyubimova, Ya.N. Parshakova, Fluid Dyn. **42**, 695 (2007).
16. S. Shklyaev, A.A. Nepomnyashchy, A. Oron, Phys. Rev. E **84**, 056327 (2011).